Building and Environment 267 (2025) 112323

Contents lists available at ScienceDirect

Building and Environment

journal homepage: www.elsevier.com/locate/buildenv

A study of gust wind speed using a novel unsteady Reynolds-Averaged Navier-Stokes model

Xiangyan Chen, Takeshi Ishihara *

Department of Civil Engineering, School of Engineering, The University of Tokyo, Tokyo 113-8656, Japan

ARTICLE INFO

Keywords:
Gust wind speed
URANS
Turbulent inflow
Averaging time
Peak factor
Skewness
Kurtosis

ABSTRACT

In this study, a novel unsteady Reynolds-Averaged Navier-Stokes (URANS) model is proposed in conjunction with a prespecified averaging time and turbulent inflow, and a new peak factor that considers the effect of averaging time used in URANS is derived to calculate gust wind speed. Firstly, the URANS incorporated with a prespecified averaging time and turbulent inflow is proposed to predict the time series of wind speed over flat terrain and investigate the variation of higher-order moments and zero-crossing rate at which the fluctuating wind speed changes algebraic sign with the averaging time. The predicted higher-order moments are less sensitive to the averaging time, but the predicted zero-crossing rate slightly decrease with increasing the averaging time due to the moving average effect. Secondly, a new peak factor is proposed to consider the averaging time. Finally, the gust wind speeds over flat terrain and around a single building predicted using the proposed URANS and the new peak factor based on the Hermite model are found to be in good agreement with the LES results, while those predicted by the conventional models deviate more from the LES results.

1. Introduction

The gust wind speed is the maximum wind speed over a short duration in a long-term wind speed time series [1]. As defined by Kristensen, the gust is the wind speed deviation from the mean which is exceeded once during the reference period [2]. Predicting gust wind speed is crucial for the design of wind turbines and buildings. Wind turbines are designed to operate within a certain range of wind speed. Gusts can impose excessive loads on the turbine blades and towers, causing structural damage or failure [3]. On the other hand, cladding of buildings in urban areas are subject to wind-induced extreme loads. Gusts can exert high wind pressures on these structures, which can lead to damage or instability [4].

As defined in IEC 61400-1 [5], gust is a temporary change in wind speed and is characterized by rise time, magnitude and duration. To accurately predict gust wind speed, it is essential in engineering applications to investigate the relationship between gust magnitude and gust duration (hereafter averaging time) [6]. According to the definition of a gust by the World Meteorological Organization [7] and IEC 61400-1 [5], the averaging time of 3 s is adopted. As stated by Burton et al. [8], the gust wind speed is affected by turbulence intensity. In addition, Hino [9] investigated the influence of various factors on the gust wind speed. The results show that the longer the averaging period of the mean wind speed T_{tot} and the shorter the averaging time t_{ave} , the greater the gust wind speed u_{max} with the averaging time of t_{ave} , whose definitions are shown in Fig. 1.

The first approach is directly calculating the gust wind speed from time series of wind speed. Ikegaya et al. [10] used Large-Eddy Simulation (LES) to predict the probabilistic characteristics of turbulent flow field in a simplified urban area. The results show that the probability distributions of wind speed tend to skew toward the direction of high wind speed regardless of the arrangement of buildings. Kikumoto et al. [11] evaluated the gust factor and peak factor based on numerical results around a single building by LES. The results indicated that both the gust factor and peak factor were high in areas with low mean wind speeds, such as at the side and back of a single building. Conversely, these factors tend to decrease in areas with high mean wind speeds. Furthermore, the uncertainty in the gust factor decreased as the mean wind speed increased, while the uncertainty in the peak factor remained constant for different wind speeds. The gust wind speeds around buildings are well predicted by LES even in regions with flow separation and reattachment, but the computational time is rather long, since a fine grid and small time step are required to achieve an accurate simulation [12].

* Corresponding author.
E-mail addresses: x.chen@bridge.t.u-tokyo.ac.jp (X. Chen), ishihara@bridge.t.u-tokyo.ac.jp (T. Ishihara).

https://doi.org/10.1016/j.buildenv.2024.112323
Received 26 August 2024; Received in revised form 21 October 2024; Accepted 15 November 2024
Available online 17 November 2024

The gust wind speed can also be calculated by multiplying the mean wind speed by the gust factor, which is efficient and fast if the mean wind speed and standard deviation are given or estimated by the Reynolds Averaged Navier-Stokes (RANS) model. Weiringa [13] fixed the averaging period at T_{tot} = 1 h and proposed an empirical formula in which the gust factor is inversely proportional to the averaging time. Furthermore, Ishizaki [14] related the gust factor to the ratio of the averaging period to the averaging time. This formula is very simple and widely used in wind engineering applications [15]. Davenport [16] derived a peak factor based on a Gaussian process to consider the effect of turbulence intensity on the gust factor and predict the peak factor based on the zero-crossing rate and averaging period. However, as stated by Holmes et al. [6], the peak factor is also a function of the averaging period and averaging time. In conclusion, the averaging period, averaging time and turbulence intensity need to be considered for the prediction of gust wind speeds, but to the best of the authors' knowledge, there are few literatures that use these parameters together.

To improve the accuracy of gust wind predictions, non-Gaussian processes were used and higher-order moments of wind speed, such as skewness and kurtosis, were incorporated into the formula predicting gust factors. Winterstein [17] developed a moment-based Hermite model to account for the significant nonlinearities of random variables, in which the nonlinear function only depends on two higher-order central moments, i.e., skewness and kurtosis [18]. The moment-based Hermite model provides a basis for establishing peak factors, but the main challenge lies in how to predict these two higher-order moments. Akahoshi et al. [19] approximated these two higher-order moments with the lower-order moment, i.e., the turbulence intensity and predicted gust wind speed using the simplified moment-based Hermite model, but the uncertainty in the proposed formula to approximate the relationship between the skewness and the turbulence intensity is relatively large. Wang and Okaze [20] used similar ideas, in which the mean wind speed and the turbulent kinetic energy are utilized to predict gust factors. The relationship between the shape parameter of the two-parameter Weibull distribution and kinetic energy ratio is established and gust wind speeds are calculated based on the exceedance probability. However, the accuracy of using lower-order moments to represent higher-order moments in these models should be investigated further.

As a bridge between LES and RANS, the unsteady Reynolds-Averaged Navier-Stokes (URANS) model can be employed to predict periodic unsteadiness caused by large-scale organized motions, such as vortex-shedding in the wake of building [21]. However, as pointed out by Ishihara and Qi [22], the performance of URANS is the same as that of RANS if a steady inflow is adopted. However, the application of URANS to predict higher-order moments and gust wind speeds has been investigated little. Therefore, a framework based on URANS is needed to predict gust wind speeds efficiently and accurately.

This study aims to propose a novel unsteady Reynolds-Averaged Navier-Stokes (URANS) model with prespecified averaging time and turbulent inflow and a new peak factor considering the averaging time to predict gust wind speeds in urban areas. Firstly, Section 2 elucidates the numerical models, including the turbulence model, generalized canopy model, turbulent inflow used in the URANS model, computational domain and grid system as well as the formulas for predicting gust wind speeds and validation metrics. Section 3 shows the performance of URANS to predict higher-order moments for different averaging times and then proposes a new peak factor considering the averaging time. Finally, the predicted gust wind speeds over flat terrain and around a single building by the proposed URANS as well as the new peak factor are validated by LES simulations. The conclusions are summarized in Section 4.

2. Numerical models and gust prediction methods

The governing equations and turbulence model used in URANS are described in Section 2.1. The turbulent inflow used in URANS simulations is presented in Section 2.2. The computational domain and grid system are given in Section 2.3. The formulas for predicting gust wind speeds and validation metrics are introduced in Sections 2.4 and 2.5.

2.1. Governing equations and turbulence model

The governing equations used in URANS are expressed by Eqs. (1) and (2) as follows:

$$\frac{\partial(\rho\widetilde{u}_i)}{\partial x_i} = 0 \tag{1}$$

$$\rho\frac{\partial\widetilde{u}_i}{\partial t} + \rho\frac{\partial\left(\widetilde{u}_j\widetilde{u}_i\right)}{\partial x_j} = -\frac{\partial\widetilde{p}}{\partial x_i} + \frac{\partial}{\partial x_j}\left[\mu\left(\frac{\partial\widetilde{u}_i}{\partial x_j} + \frac{\partial\widetilde{u}_j}{\partial x_i}\right)\right] - \rho\frac{\partial\widetilde{u_i u_j}}{\partial x_j} + f_{\widetilde{u},i} \tag{2}$$

where $\widetilde{u}_i(t)$ is the resolved velocity in the i direction (i = 1, 2, 3) and $\widetilde{p}$ is the resolved pressure. ρ is the air density and μ is the molecular viscosity. $f_{\widetilde{u},i}$ is the fluid force caused by vegetation and buildings. The stress $\widetilde{u_i u_j}$ in Eq. (2) is usually modelled by eddy-viscosity hypothesis and is expressed as,

$$\widetilde{u_i u_j} = 2\mu_t\widetilde{S}_{ij} + \frac{\delta_{ij}}{3}\widetilde{u_k u_k} \tag{3}$$

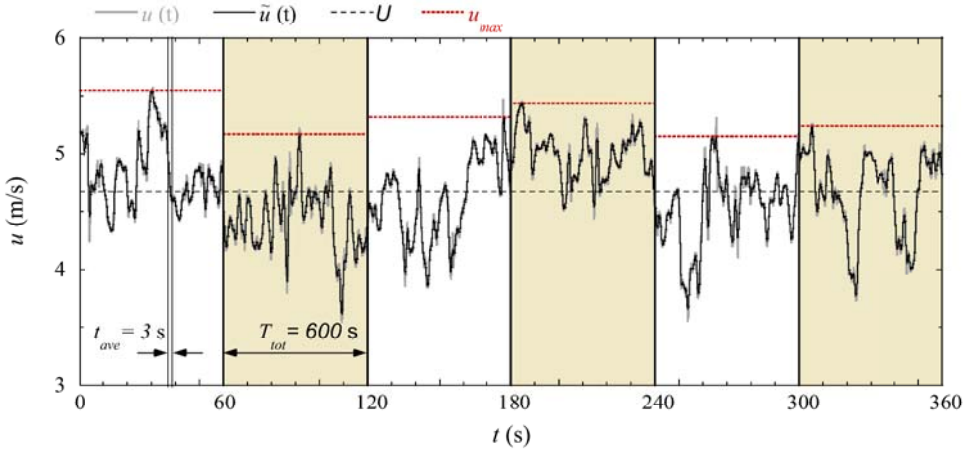

Fig. 1. Schematic diagram of nomenclatures related to gust wind speeds; $\boldsymbol{u}(\boldsymbol{t})$ is the instantaneous velocity, $\widetilde{\boldsymbol{u}}(\boldsymbol{t})$ is the moving averaged velocity with averaging time of $\boldsymbol{t_{ave}}$ = 3 s and $\boldsymbol{U}$ is the long-term mean velocity with $\boldsymbol{T_{tot}}$ = 600 s.

$$\widetilde{S}_{ij} = \frac{1}{2}\left(\frac{\partial \widetilde{u}_i}{\partial x_j} + \frac{\partial \widetilde{u}_j}{\partial x_i}\right) \tag{4}$$

where δ_{ij} is the Kronecker delta function. μ_t is the turbulence viscosity and can be written as,

$$\mu_t = C_\mu \rho \frac{k_S^2}{\varepsilon_S}. \tag{5}$$

where k_S and ε_S are the modelled turbulent kinetic energy and turbulent dissipation rate, which are computed from the transport equations in the STRUCT k-ε model by Xu [23] as follows:

$$\frac{\partial \rho k_S}{\partial t} + \frac{\partial \rho \widetilde{u}_j k_S}{\partial x_j} = \frac{\partial}{\partial x_j}\left[\left(\mu + \frac{\mu_t}{\sigma_k}\right)\frac{\partial k_S}{\partial x_j}\right] - \rho \widetilde{u_i u_j}\frac{\partial \widetilde{u}_j}{\partial x_i} - \rho \varepsilon_S \tag{6}$$

$$\frac{\partial \rho \varepsilon_S}{\partial t} + \frac{\partial \rho \widetilde{u}_j \varepsilon_S}{\partial x_j} = \frac{\partial}{\partial x_j}\left[\left(\mu + \frac{\mu_t}{\sigma_\varepsilon}\right)\frac{\partial \varepsilon_S}{\partial x_j}\right] - C_{\varepsilon 1}\rho \widetilde{u_i u_j}\frac{\partial \widetilde{u}_j}{\partial x_i}\frac{\varepsilon_S}{k_S} - C_{\varepsilon 2}\frac{\rho \varepsilon_S^2}{k_S} - \frac{C_\mu \rho \eta^3 \left(1 - \frac{\eta}{\eta_0}\right)}{1 + \beta \eta^3}\frac{\varepsilon_S^2}{k_S} + S_\varepsilon, \tag{7}$$

where σ_k and σ_ε are the inverse effective Prandtl numbers for k_S and ε_S, respectively. The default constants in transport equations are $C_{\varepsilon 1} = 1.42$, $C_{\varepsilon 2} = 1.68$, $C_{\varepsilon 3} = 1.5$, $C_\mu = 0.0845$, $\sigma_k = \sigma_\varepsilon = 1.393$. These parameters are default values in Fluent [24] and are used to simulate the neutral atmospheric boundary layer.

Compared to the standard k-ε model, the STRUCT k-ε model includes two additional source terms on the right-hand side of Eq. (7). The fourth term is from the conventional RNG k-ε model by Yakhot et al. [25] and is used to describe the effects of rapid strain and streamline curvature, in which $\eta_0 = 4.38$, $\beta = 0.012$. $\eta \equiv |\widetilde{S}|k_S/\varepsilon_S$ and $|\widetilde{S}| = \sqrt{\widetilde{S}_{ij}\widetilde{S}_{ij}}$. The fifth term S_ε in Eq. (7) is the product of a constant $C_{\varepsilon 3}$, turbulent kinetic energy $\widetilde{k}$ and the second invariant of the resolved velocity gradient tensor, $\widetilde{II}$ used to describe regions lack applicability of the scale-separation assumption in Xu [23] as follows:

$$S_\varepsilon = C_{\varepsilon 3} k_S \widetilde{II} = -\frac{C_{\varepsilon 3} k_S}{2}\frac{\partial \widetilde{u}_i}{\partial x_j}\frac{\partial \widetilde{u}_j}{\partial x_i} \tag{8}$$

The constant $C_{\varepsilon 3}$ of 1.5 is determined by a sensitivity study by Xu [23] and is used to predict the flow fields around the freight train and T-junction by Garcia et al. [26] and Feng et al. [27]. By including the source term in Eq. (7), the resolved frequencies are always smaller than the modelled frequencies and therefore the velocity fluctuations are captured even for large time steps. In this way, URANS used in this study overcomes the overestimation of turbulence viscosity in the wake region and decays at the smallest scales.

In this study, the turbulent flow field around a single building is investigated using the canopy model as source terms to calculate the momentum caused by the building in the turbulent boundary layer. Enoki and Ishihara [28] and Ishihara et al. [29] proposed a generalized canopy model considering both vegetation and buildings by adding a fluid force, $f_{\widetilde{u},i}$, in Eq. (2).

$$f_{\widetilde{u},i} = \frac{F_{\widetilde{u},i}}{V_{grid}} = -\frac{1}{2}\rho C_f \frac{\gamma_0}{l_0}|\widetilde{u}|\widetilde{u}_i \tag{9}$$

$$l_0 = \frac{4V_b}{S_b}, C_f = \frac{C_{D,b}}{(1-\gamma_0)^3} = \frac{1}{(1-\gamma_0)^3}\min\left[\frac{1.53}{1-\gamma_0}, 2.75(1-\gamma_0)\right] \tag{10}$$

where V_{grid} is the grid volume. $|\widetilde{u}|$ is the absolute value of resolved velocity and $\widetilde{u}_i$ is the resolved velocity in the i direction. γ_0 is the packing density and l_0 is the representative length scale of buildings. V_b and S_b are the volume and total side surface of buildings, respectively. C_f is the equivalent drag coefficient and $C_{D,b}$ is the drag coefficient of buildings.

The finite volume method is employed to discretize the governing equations of continuity and momentum. Numerical simulations are conducted using Fluent [24]. The spatial discretization method is second order upwind. A second-order implicit scheme is utilized for time discretization. Pressure-velocity coupling is implemented using the Semi-Implicit Pressure Linked Equations (SIMPLE) approach. Pressure outlet boundary conditions are set at the outlet. Symmetrical conditions are imposed on the side and top boundaries. The bottom surface is modeled as a non-slip wall with a surface roughness of $z_0 = 0.018$ m in real scale, consistent with the setup of the experiment by Meng and Hibi [30].

In this study, the mean velocity U and standard deviation σ_u^2 in the streamwise direction are calculated as follows:

$$U = \overline{\widetilde{u}}, \sigma_u^2 = \overline{u'^2} + \overline{\widetilde{u}\widetilde{u}} \tag{11}$$

where $\overline{\widetilde{u}}$ is the mean value of the resolved velocity $\widetilde{u}$, σ_u^2 is the standard deviation, obtained from the fluctuating resolved velocity $u' = \widetilde{u} - U$ and the modelled turbulence $\overline{\widetilde{u}\widetilde{u}}$. V and σ_v^2 in the spanwise direction as well as W and σ_w^2 in the vertical direction can be calculated similarly.

2.2. Generation of turbulent inflow for URANS

For the turbulent inflow, according to Irwin [31], the spire with height of 0.6m and fence with height of 0.1 m is used to reproduce the neutrally stratified atmospheric boundary layer in the wind tunnel test by Meng and Hibi [30]. To adjust the wind fields near the ground, cubic blocks with heights of 0.06 m, 0.02 m and 0.01 m are set in sequence at 0.21 m downstream of the fence. Based on the width of the single building and the velocity at the height of the building, the Reynolds number is 2.4×10^4. The turbulent inflow is generated by the spire, fence and cubic blocks as shown in Qi and Ishihara [32]. The predicted vertical profiles of mean wind velocity and turbulence intensity can be expressed by those of terrain subcategory V defined by the AIJ [33].

At the inlet boundary of the URANS model, the turbulent inflow based on the dataset of $u_i(t)$ generated by the LES simulation using above configuration is separated into two parts: resolved turbulence and modelled turbulence as shown in Fig. 2. This is achieved by defining a specific averaging time. The reason why the averaging time allows separation of turbulence into resolved and modelled components is that the averaging time proposed in this study is related to the window width of the low-pass filter. As pointed out by Israel [34], filtering a fully resolved turbulent field with any low-pass filter characterized by a specified length scale results in a filtered velocity field, where unsteady fluctuating terms can be introduced to the initial conditions. Therefore,

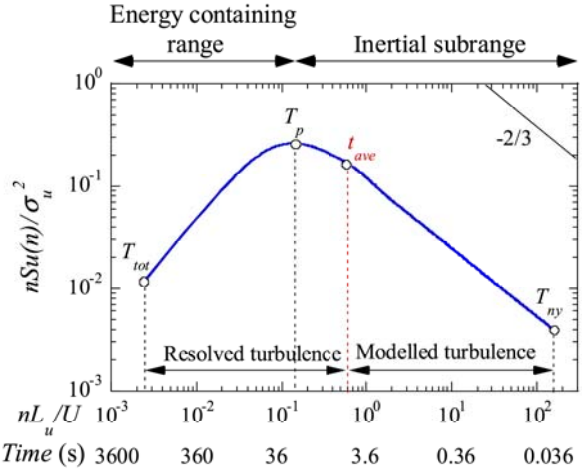

Fig. 2. Schematic of power spectral density of streamwise velocity component and nomenclatures used for gust wind speed prediction.

the subgrid cutoff of URANS depends on the proposed averaging time.

In Fig. 2, T_p is the peak period corresponding to peak frequency and T_{ny} is the time corresponding to the Nyquist frequency. To generate turbulent inflow, the averaging time normalized by the peak period is called γ_t and calculated as follows:

$$\gamma_t = \frac{t_{ave}}{T_p} \tag{12}$$

where the averaging time t_{ave} is located between T_{tot} and T_{ny}. The peak period T_p is calculated from the spectrum of the reference wind speed at the height of 160 m and is 30 s corresponding to the wind tunnel test by Meng and Hibi [30]. When $\gamma_t > 1$, the performance of URANS is close to RANS. Conversely, when $\gamma_t < 1$, URANS can capture the small-scale vortices as shown in Fig. 3. The vortex structures in Fig. 3 are visualized by λ_2 method as shown in Jeong and Hussain [35]. As γ_t increases from 1/30 to 1/3 according to the averaging time from 1 sto 10 s, the small-scale vortices decrease, i.e., the proportion of resolved turbulence decreases. Therefore, the averaging time must be within a certain range to capture coherent structures in the turbulent flow field if the purpose of the URANS simulation is to predict gust wind speeds.

The resolved and modelled turbulence are obtained by applying a moving average to the dataset. The window width of the moving average d is,

$$d = 2t_{ave}/dt \tag{13}$$

where dt is the time interval of the dataset of $u_i(t)$. For example, when the time interval $dt = 0.01$ s and $t_{ave} = 10$ s are selected, the window width dw of the moving average is 2000.

The instantaneous resolved velocity, instantaneous modelled turbulent kinetic energy and turbulent dissipation rate are calculated as follows:

$$\widetilde{u}_{i,j} = \frac{1}{d+1}\sum_{j-d/2}^{j+d/2} u_{ij} \tag{14}$$

$$k_{s,j} = \frac{1}{2}\sum_{i=1}^{3}\left(\frac{1}{d+1}\sum_{j-d/2}^{j+d/2}\left(u_{ij} - \widetilde{u}_{ij}\right)^2\right) \tag{15}$$

$$\varepsilon_{s,j} = \frac{C_\mu^{3/4} k_{s,j}^{3/2}}{\kappa z'} \tag{16}$$

where $u_{i,j}$ is the *jth* data of the dataset $u_i(t)$ in the i direction, $\widetilde{u}_{i,j}$ is the corresponding resolved velocity. $k_{s,j}$ and $\varepsilon_{s,j}$ are the modelled turbulent kinetic energy and turbulence dissipation rate, respectively. After the velocity from the dataset is separated into resolved and modelled components, the time series of resolved velocity, modelled turbulent kinetic energy and modelled turbulence dissipation rate are imported to each grid at the inlet boundary.

2.3. Computational domain and grid system used in URANS

In this study, the gust wind speeds over flat terrain are first investigated. Fig. 4 (a) shows a bird's eye view of the computational domain. The domain size is $90h(x) \times 16.5h(y) \times 22.5h(z)$ and h is a representative height of 0.04 m, which is same as that by Ishihara and Qi [22]. The inlet boundary is $30h$ upstream from the center of target and the turbulent inflow is generated using the dataset of $u_i(t)$ as described in Section 2.2. The downstream space is extended by $60h$. Fig. 4 (b) presents a top view of the grid system of the entire computational domain. Fig. 4 (c) and (d) depict the target zone and the grid system in detail. A grid size of 1.0 mm is used in the target region in this study. To control the grid quantity and enhance computational efficiency, a hybrid grid system used by Ishihara and Qi [22] is employed. In Fig. 4 (b), the red rectangle marks the target zone with a grid size of 1 mm. Surrounding the target zone, elongated yellow rectangles serve as buffer zones, where triangular grids facilitate a gradual transition from fine to coarse grids. Upstream of the target zone, the grid size is 10 mm, while the grid size above and below the target zone is 8 mm. This computational domain and grid system is used to generate the turbulent flow field over flat terrain by URANS with a prespecified averaging time.

In this study, the gust wind speeds around a single building are then studied. The size of the single building is $B \times B \times H$ ($H = 2B = 0.16$ m) in the streamwise, spanwise and vertical directions as shown in Fig. 5 (a), which is the same as the single building used in the wind tunnel test conducted by Meng and Hibi [30]. In this simulation, the URANS model is used, and the turbulent inflow is generated using the dataset of $u_i(t)$ as described in Section 2.2. The configuration of the computational domain is illustrated in Fig. 5 (b). The width and height of the computational domain are 1.1 m and 0.9 m. The distances from the center of the building to the inlet and outlet boundaries are $3.1H$ and $15.0H$, respectively. As shown in Fig. 5 (b), a fine grid resolution is employed near the ground, gradually transitioning to a coarser grid in the upper layer. The minimum vertical grid resolution is set to 0.005 m, while the maximum vertical grid resolution is no more than 0.03 m. Specifically a structural grid with a horizontal resolution of 0.004 m is implemented around the single building. The vertical grid resolution varies from a minimum of 0.002 m at the bottom of the building and a maximum of 0.01 m at the top of the building.

To simplify the grid system of the computational domain, the generalized canopy model introduced in Section 2.1 is used to simulate the impact of the single building on the surrounding wind field. The representative length scale, packing density and equivalent drag coefficient of the cubic blocks and the single building calculated using Eq. (9) are summarized in Table 1.

2.4. Prediction of gust wind speeds

To consider the significant nonlinearities of random variables, Winterstein [17] proposed a moment-based Hermite model. In this

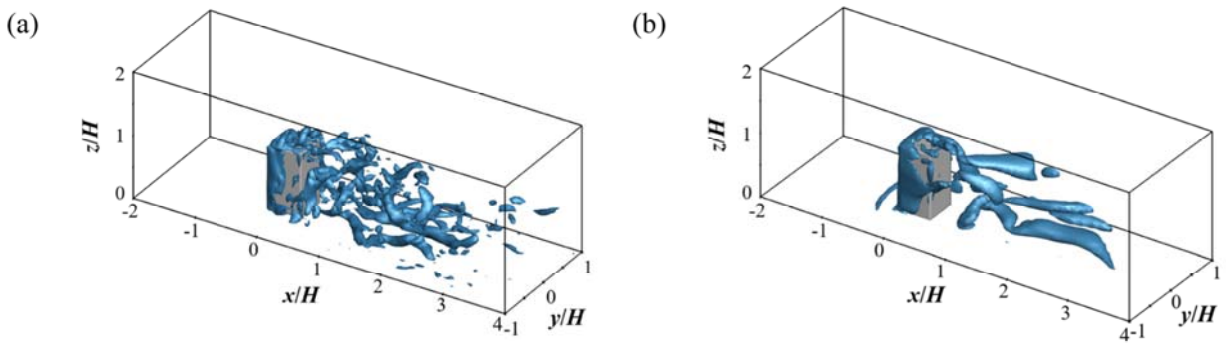

Fig. 3. Vortices around a single building by URANS with normalized averaging time (a) $\gamma_t = 1/30$ and (b) $\gamma_t = 1/3$ visualized with $\lambda_2 = -10{,}000$.

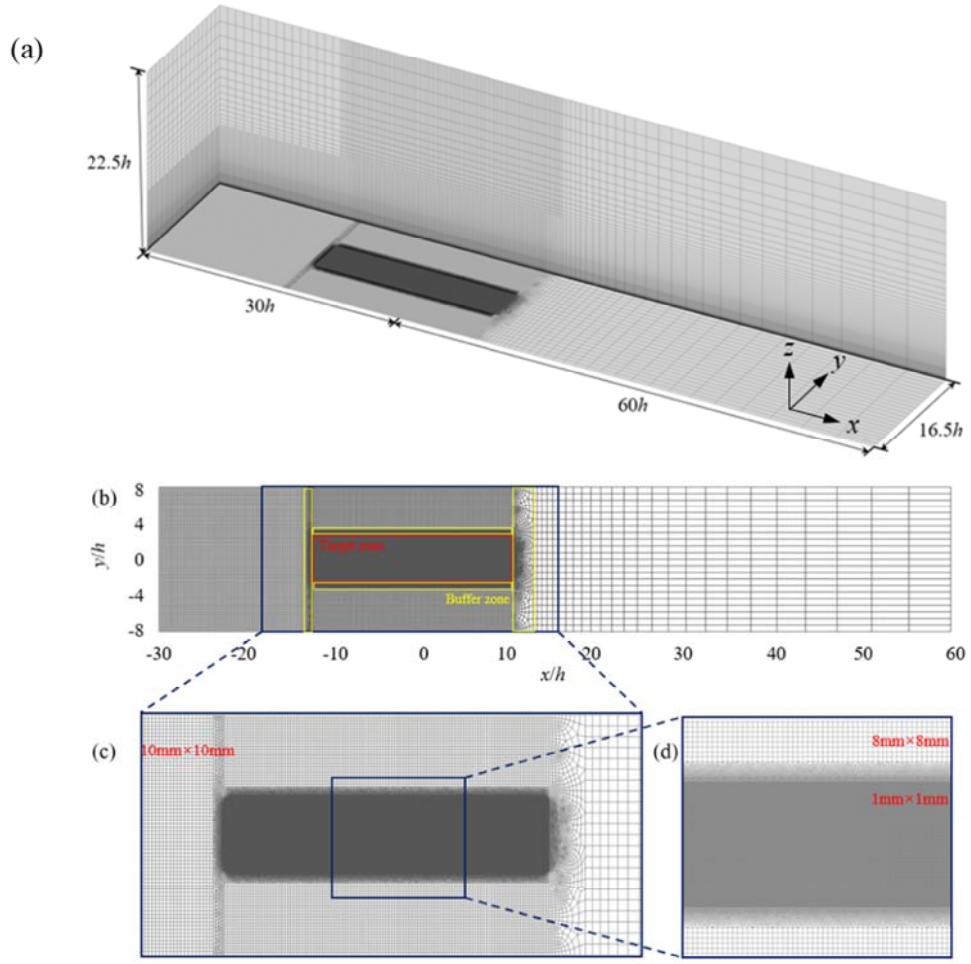

Fig. 4. Grid system and computational domain for flat terrain: (a) bird's eye view of the computational domain, (b) top views of entire area, (c) target zone and (d) grid system in detail. ***h*** is a representative height of 0.04 m.

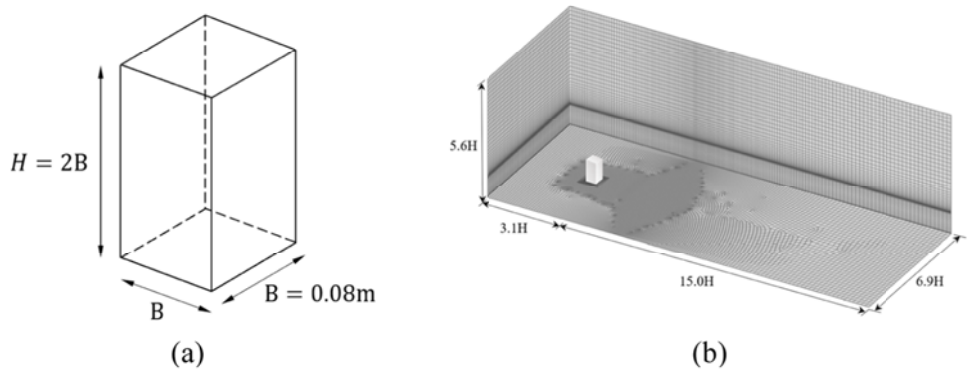

Fig. 5. Configuration of the computational domain for a single building: (a) size of the single building, (b) bird's eye view of hybrid system.

Table 1
Summary of parameters of canopy models for approximations of cubic blocks and a single building.

Canopy	Representative length scale, l_0 (m)	Packing density, γ_0 (%)	Equivalent drag coefficient, C_f
Block 1	0.06	6.25	1.981
Block 2	0.02		
Block 3	0.01		
Single building	0.08	99.9999	2.75×10^{12}

study, the gust wind speed u_{max} in the streamwise direction is predicted based on the modified Hermite model using the mean speed U, standard deviation σ_u and peak factor g as:

$$u_{max} = UG_{max} = U \pm g\sigma_u \tag{17}$$

The peak factor g is expressed using the Hermite coefficients h_3, h_4 and a dimensionless factor X with a correction coefficient $f(t_{ave}/T_{tot})$ as follows:

$$g = \kappa\left[X + h_3\left(X^2 - 1\right) + h_4\left(X^3 - 3X\right)\right] f(t_{ave}/T_{tot}) \tag{18}$$

$$h_3 = \frac{\alpha_3}{6 + 2\sqrt{1 + 1.5(\alpha_4 - 3)}} \tag{19}$$

$$h_4 = \frac{\sqrt{1 + 1.5(\alpha_4 - 3)} - 1}{18} \tag{20}$$

$$\kappa = \frac{1}{\sqrt{1 + 2h_3^2 + 6h_4^2}} \tag{21}$$

where h_3 and h_4 are calculated by skewness α_3 and kurtosis α_4. κ is the scaling factor. $f(t_{ave}/T_{tot})$ is a correction coefficient discussed in Section 3.2 and expressed as a function of the averaging time t_{ave} normalized by the averaging period T_{tot} of 600 s. Note that Eq. (18) expresses the original moment-based Hermite model if $f(t_{ave}/T_{tot}) = 1$.

The dimensionless factor X is a function of the zero-crossing rate ν_u^+ and the averaging period T_{tot}, and calculated as follows:

$$X = \sqrt{2\ln\left(\nu_u^+ T_{tot}\right)} \tag{22}$$

The zero-crossing rate ν_u^+ is expressed as:

$$\nu_u^+ = \frac{1}{\kappa\sqrt{1 + 4h_3^2 + 18h_4^2}} \frac{\sqrt{\int_{-\infty}^{\infty} f^2 S_u(f)df}}{\sqrt{\int_{-\infty}^{\infty} S_u(f)df}} \tag{23}$$

where S_u is the power spectral density of the streamwise velocity u. The gust wind speeds in the spanwise and vertical directions can be calculated similarly. Eqs. (17)–(23) are formulas to predict gust wind speed using URANS that take turbulent inflow into account, and $S_u(f)$ refers to the power spectral density obtained from URANS.

Higher-order moments can be accurately predicted by LES using fine grids and small time steps, but the computational time is very long. In contrast, RANS lacks the ability to predict spectra or higher-order moments but is computationally efficient and widely used in wind engineering applications. Recently, several models have been proposed to predict gust wind speeds using lower-order moments obtained from RANS, such as turbulence intensity or kinetic energy ratio to approximate higher-order moments. Akahoshi et al. [19] proposed formulas to estimate higher-order moments using turbulence intensity, however, it was based on field observations. This method is called the Akahoshi model and is described in detail in Appendix A in detail. Meanwhile, Wang and Okaze [20] assumed that the velocity distribution follows a two-parameter Weibull distribution and expressed the shape parameter of the Weibull distribution as a function of the kinetic energy ratio. This method is named the W&O model and is explained in Appendix B in detail.

2.5. Validation metrics

In this study, the evaluation of the accuracy of the proposed modified Hermite model, Akahoshi and W&O models is based on the hit rate q, which was introduced in previous studies [22,36,37] and expressed as follows:

$$q = \frac{1}{N}\sum_{i=1}^{N} n_i, with\ n_i = \begin{cases} 1, \left|\frac{y-x}{x}\right| \le D_q\ or\ |y-x| \le 0.05|max| \\ 0, else \end{cases} \tag{24}$$

where x and y are the measured and predicted variables. N represents the total number of measured or simulated values. $D_q = 0.15$ [22] is adopted in this study. $|max|$ represents the maximum value of the measured and simulated results. The hit rate is taken to represent the fraction of cases where y is within 15 % of x or their difference is less than 5 % of the maximum. This metric is employed to assess the performance of the models in predicting gust wind speeds.

3. Results of gust wind speed prediction

The performance of URANS to predict higher-order moments is illustrated in Section 3.1. A correction coefficient that considers the effect of averaging time is proposed in Section 3.2 and is then validated using the turbulent flow fields over flat terrain and around a single building in Section 3.3.

3.1. Evaluation of higher-order moments

To determine the length scale and time scale of the numerical simulation, the vertical profiles of mean wind speed and turbulence intensity obtained from the LES simulation with a wind speed of 6 m/s at the height of 0.16 m are fitted to the vertical profiles of different terrain subcategories defined in AIJ [33].

The results show that the generated turbulent wind field at $z/H \le 2.0$ are close to terrain subcategory V in AIJ [33] as shown in Fig. 10, and the length scale is determined to be 1:1000. Since the velocity scale is arbitrary, it is set as 1:10 in this study and the time scale is determined to be 1:100 to fit the power spectral density of streamwise velocity. The reference height H and reference wind speed U_{ref} in real scale are calculated to be 160 m and 60 m/s, respectively. The various scales and reference values used in this study are summarized in Table 2.

Fig. 6 shows an example of power spectral density of streamwise velocity at the reference height, H = 165 m, The Kaimal spectrum as shown in IEC 61400-1 [5] and the averaging times of 2, 3, 5 and 10 s are also plotted in Fig. 6 for comparison. The LES simulation can accurately capture high-frequency fluctuations around 3 s in the inertial subrange, but fluctuations shorter than 3 s are smoothed due to the limitation of grid resolution [20]. As t_{ave} moves from the right to the left as illustrated in Fig. 6, the fraction of the resolved turbulence decreases, but that of modelled turbulence increases. In this study, different averaging times of t_{ave} = 3, 5 and 10 s and a fixed averaging period of T_{tot} = 600 s are used to investigate their impact on the peak factor.

To evaluate the effects of averaging time on evaluation of higher-order moments, the LES results are smoothed and used to calculate higher-order moments and zero-crossing rates. Fig. 7 presents variation of higher-order moments and zero-crossing rate with different averaging time t_{ave} from 3 to 10 s. It can be observed that the mean wind speed and standard deviation normalized by U_{ref}, skewness and kurtosis are not sensitive to the averaging time. This is because the first four moments are long-term statistics and are stable rather than short-term fluctuations. These statistics are influenced by the large-scale turbulence structures and are less affected by the change in resolution of gust events captured with different averaging times. From the perspective, URANS can provide accurate higher-order moments even when the averaging time is large and the computational time can be significantly reduced, since the higher-order moments are insensitive to the averaging time. However, as t_{ave} increases, the zero-crossing rate decreases because more data are averaged over a longer period. This smoothing effect reduces the amplitude of the fluctuating velocity. Consequently, the number of crossings on the time axis (zero-crossing) decreases because the rapid fluctuations that cause frequent zero crossings are reduced by the moving average process. Therefore, a modified Hermite model is needed for larger averaging times, and the correction coefficient as shown in Eq. (18) in Section 2.4 needs to be identified.

Table 2
Description of various scales and reference values used in this study.

Item	Prototype	Model
Length scale	1	1/1000
Velocity scale	1	1/10
Time scale	1	1/100
Reference height H (m)	165	0.165
Reference wind speed U_{ref} (m/s)	60	6

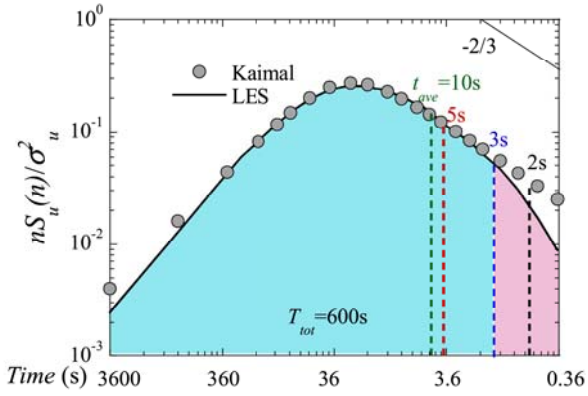

Fig. 6. Power spectral density of streamwise velocity at the reference height H = 165 m with averaging time t_{ave} = 3 s, 5 s and 10 s and a fixed averaging period of T_{tot} = 600 s.

3.2. Correction coefficient of peak factor

To evaluate the peak factor in Eq. (18), the parameter X consisting of the zero-crossing rate ν_u' and the averaging period T_{tot} needs to be calculated. In this study, the correction coefficient $f(t_{ave}/T_{tot})$ is identified by dividing the peak factor calculated using LES results by those calculated using the original Hermite model to propose a new peak factor that is independent of the averaging time used in the URANS model as shown in Eq. (25).

$$f(t_{ave}/T_{tot}) = 1.6e^{-0.2(t_{ave}/T_{tot})} - 0.6e^{-165(t_{ave}/T_{tot})},\ T_{tot} = 600\ \text{s} \tag{25}$$

The correction coefficient is based on the methodology of Hino [9], who parameterized the effect of a short-term moving average on the long-term moving average derive the formula for gust factor. In this study, the same idea is adopted to correct the formula for the peak factor and the correction coefficient in Eq. (25) is empirically derived as a function of t_{ave}/T_{tot}.

Fig. 8 shows the variation of the correction coefficients with respect to the averaging time t_{ave}. The predicted correction coefficient approaches to 1 when the averaging time is close to 0. The peak factor

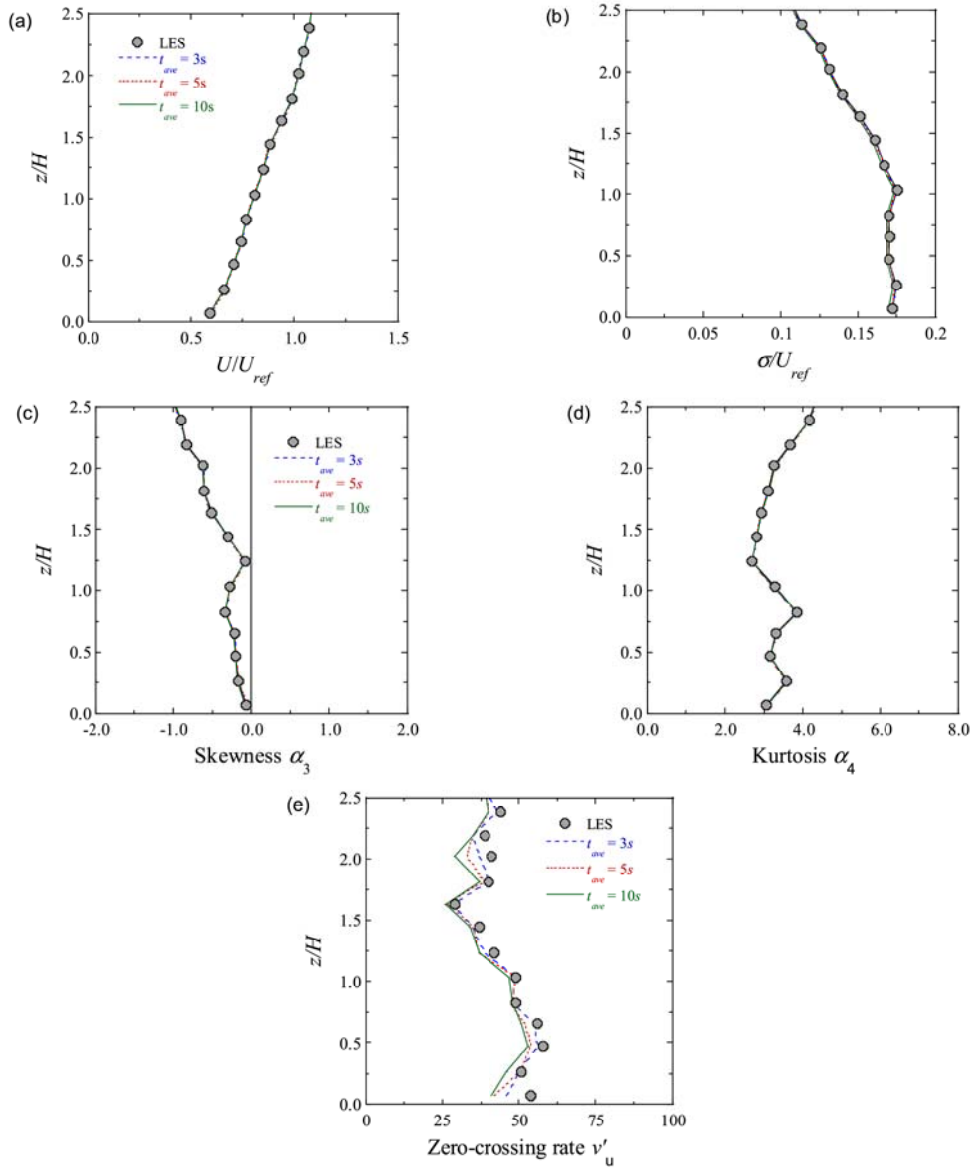

Fig. 7. Variations of (a) mean wind speed, (b) standard deviation, (c) skewness, (d) kurtosis, (e) zero-crossing rate for the flat terrain obtained from URANS with averaging time t_{ave} = 3 s, 5 s and 10 s.

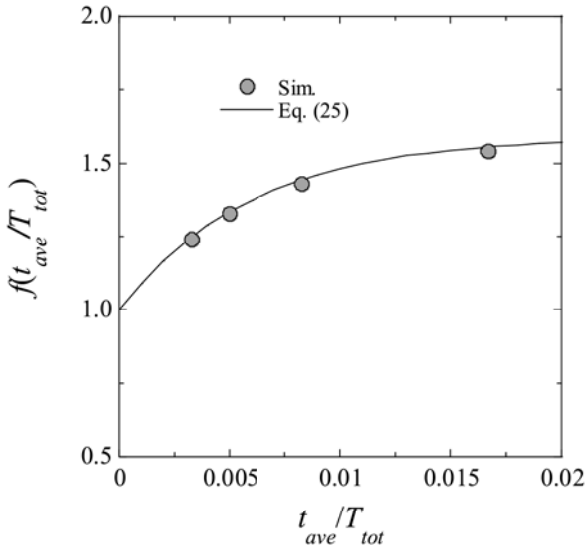

Fig. 8. Variation of correction coefficients that corrects the Hermite model with the averaging time.

shown in Eq. (18) can be calculated using the correction coefficient in Eq. (25) that considers the effect of the averaging time. Therefore, the gust wind speed that is not affected by the averaging time can be evaluated using Eq. (17). As shown in Fig. 6, the peak velocity from the LES can capture high-frequency fluctuations around 3 s due to the limitation of grid resolution [20]. As a result, u_{max} evaluated using Eq. (17) corresponds to the gust wind speed for almost 3 s.

To demonstrate the accuracy improvement with the modified Hermite model, Fig. 9 shows the vertical profiles of the peak factors predicted by the original and modified Hermite models. The peak factors predicted by the modified Hermite model show almost the same values and are independent of the averaging time, while the original Hermite model underestimates the peak factors obtained from LES because the streamwise velocity is smoothed using a longer averaging time.

The advantage of the proposed method is that it can accurately predict the turbulence intensity at large time steps, since the total turbulence kinetic energy does not change with the averaging time, i.e. the time step. On the other hand, LES cannot accurately predict gust wind speeds at large time steps, since the resolved turbulence is underestimated. The differencing schemes used in URANS may affect the correction coefficient. Seng et al. [38] concluded that a temporal scheme of at least second order is required to accurately discretize the unsteady terms in the governing equations. In addition, the pressure-velocity coupling used in this study is the Semi-Implicit Pressure Linked Equations (SIMPLE) approach. As stated by Hadi et al. [39], the SIMPLE method can reach acceptable convergence for the simulation of Karman vortex that occurs in the turbulent flows around mountains and islands. As a result, URANS gives the same results as LES for the same small time-step and the influence of the differencing schemes on the correction coefficient is expected to be limited.

3.3. Validation and discussion

Figs. 10 and 11 show the vertical profiles of mean wind speed and turbulent kinetic energy over flat terrain and around the single building predicted by URANS, which are compared with the LES results and the wind tunnel experiments by Meng and Hibi [30]. In this study, the time step Δt in URANS simulations is the same as the averaging time t_{ave}.The time step used in URANS are 10 s, while the time step in LES is 0.01 s to satisfy the Courant Friendrichs Lewy (CFL) condition [40]. The vertical profiles of mean streamwise velocity and turbulent kinetic energy by the proposed URANS model are in good agreement with those obtained from the wind tunnel experiment [30] even with the averaging time of 10 s. The highest mean streamwise velocity and turbulent kinetic energy occurs in the shear layer above the building as shown in Fig. 11. The flow separation and reattachment are also well captured by the proposed URANS model. The prediction accuracy of URANS is almost the same as that of the LES simulation, indicating that the proposed method has high computational efficiency in engineering applications.

To evaluate the performance of the proposed model shown in Eq. (18), the vertical profiles of normalized gust wind speed over flat terrain predicted by the proposed modified Hermite model, Akahoshi and W&O models are first compared in Fig. 12 (a), where U_{ref} is the reference velocity at the reference height of 160 m. In this study, this height is the same as the building height. The mean streamwise velocity and standard deviation obtained from the LES simulation are used in the Akahoshi and W&O models to clarify the accuracy of the two models for predicting peak factors. The validation metrics of the predicted and simulated gust wind speeds are shown in Fig 12 (b). It can be observed that all of the points from the proposed model are within the blue thresholds, while some of the points from the Akahoshi model are above the thresholds and some of the points from the W&O model are below the thresholds. To quantitively evaluate the accuracy of the three models, the hit rates of gust wind speeds predicted by the proposed Hermite model, Akahoshi and W&O models are calculated, which are 1.00, 0.69 and 0.75, respectively. The predicted gust wind speeds by the proposed model are in good agreement with those by the LES simulation, while the gust wind speeds obtained by the Akahoshi model are overestimated and the gust wind speeds predicted by the W&O model are underestimated. The hit rate of the proposed model shows the highest value among the three models.

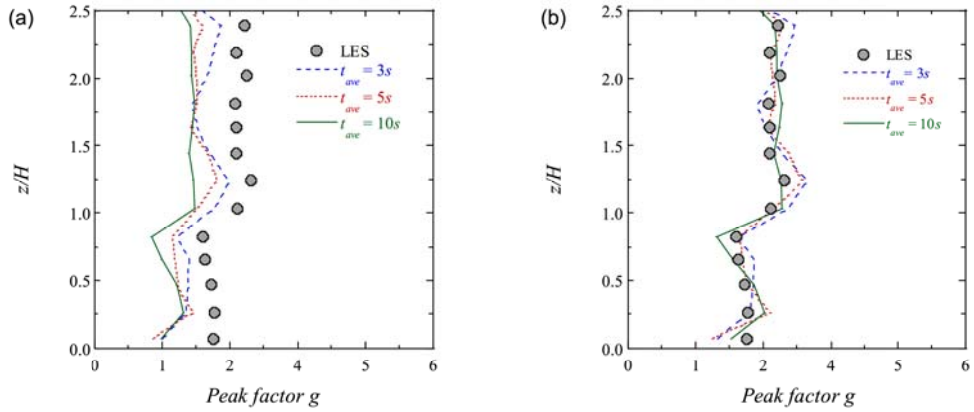

Fig. 9. Comparison of peak factors with averaging time t_{ave} = 3 s, 5 s and 10 s predicted by (a) original Hermite model, (b) modified Hermite model with correction coefficients.

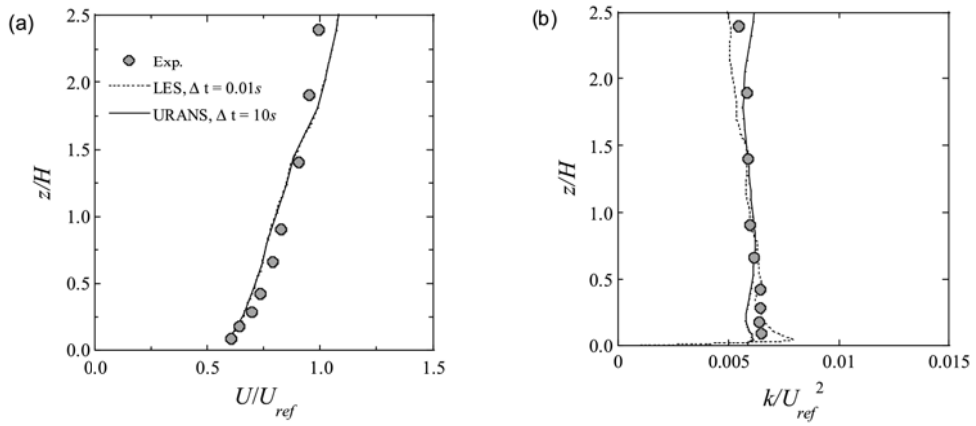

Fig. 10. Vertical profiles of (a) mean wind speed and (b) turbulent kinetic energy over flat terrain by LES with time step $\Delta t = 0.01$ s and URANS with time step $\Delta t = 10$ s.

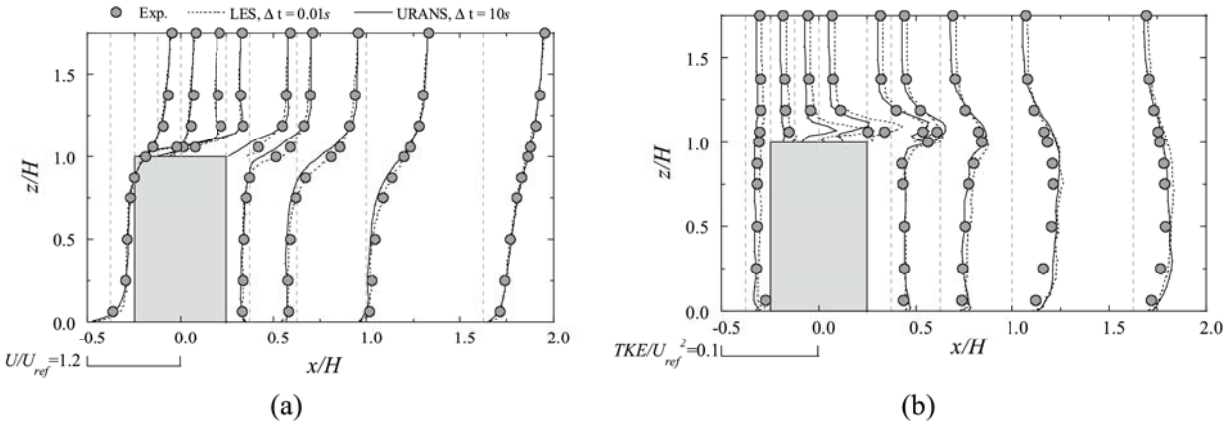

Fig. 11. Vertical profiles of (a) mean wind speed, (b) turbulent kinetic energy around the single building by LES with time step $\Delta t = 0.01$ s and URANS with time step $\Delta t = 10$ s.

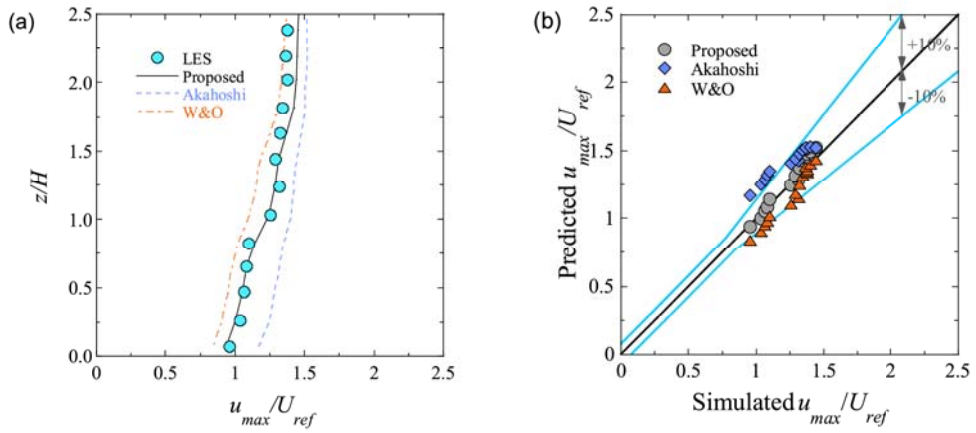

Fig. 12. Comparison of normalized gust wind speed over flat terrain predicted by the proposed model with $t_{ave} = 10$ s, Akahoshi and W&O models: (a) vertical profiles, (b) validation metrics.

To clarify the model performances, the skewness and kurtosis predicted by the proposed modified Hermite model with $t_{ave} = 10$ s, Akahoshi and W&O models are illustrated in Fig. 13. The overestimation of gust wind speed by the Akahoshi model is mainly caused by the inherent uncertainty in the relationship between skewness and turbulence intensity. Meanwhile, the underestimation of gust wind speed by the W&O model is because the kinetic energy ratio over flat terrain is much smaller than that in the wind fields around a building. The hit rates of skewness by the proposed modified Hermite model, Akahoshi and W&O models over flat terrain are 1.00, 0.69 and 1.00, while the hit rates of kurtosis are 1.00, 0.77 and 0.85. The hit rates of higher-order moments predicted by the proposed model are the highest, followed by the W&O model and the Akahoshi model.

The accuracy of the predicted peak factors around a single building

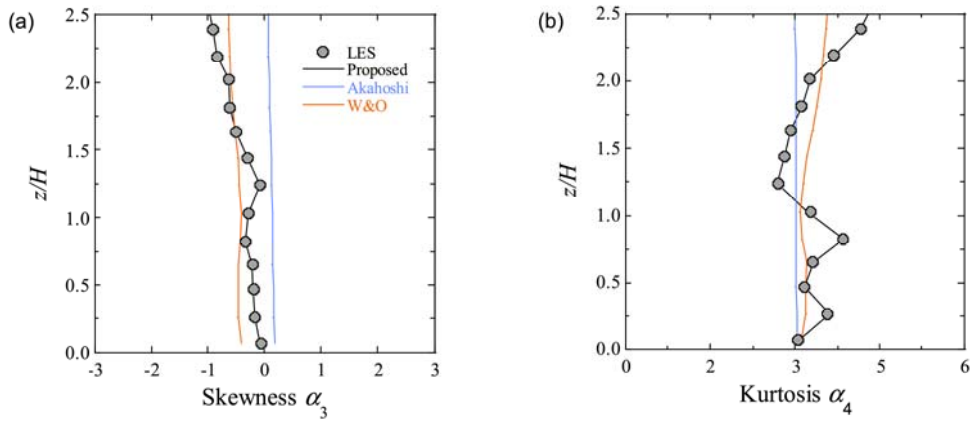

Fig. 13. Comparison of higher-order moments, (a) skewness and (b) kurtosis, of wind speed, predicted by the proposed model with t_{ave} = 10 s, Akahoshi and W&O models.

by the proposed model is examined. The peak factors from LES are obtained using the time series data of streamwise velocity. The points shown in Fig. 14 are selected around the single building on the vertical plane of $y/H = 0$, and horizontal plane of $z/H = 0.0625$ to record instantaneous streamwise velocity.

The gust wind speed in the vertical and horizontal planes predicted by the LES simulation and the proposed model are visualized by the contours in Fig. 15. In the horizontal plane, the contours of gust wind speeds by the proposed model agree well with those predicted by the LES simulation, as shown in Fig. 15 (b) and (d). On the other hand, in the vertical plane, the gust factors predicted by the proposed model are slightly overestimated compared to those by LES. This is because the streamwise and spanwise wind speeds in the horizontal plane are the most dominant when the model is proposed to evaluate the pedestrian-level gust wind speeds, as shown by the studies of Shirzadi and Tominaga [41] and Li et al. [42]. In addition, few studies have compared the predicted gust wind speeds in the vertical plane with those from LES. Although the gust wind speed by the proposed model is slightly overestimated in the vertical plane compared to LES, the overall distribution of gust wind speed is very similar to that by LES.

For quantitative comparison, the validation metrics of predicted gust wind speeds by the proposed model and the W&O model are plotted in Fig. 16. Most of the predicted gust wind speeds at the selected points by the proposed modified Hermite model fall within the borderlines of the validation metrics, while some of the predicted gust wind speeds by the W&O model are underestimated, which is also observed by Wang and Okaze [20]. The reason is that the shape parameter of the Weibull distribution is overestimated due to the increase in the mean kinetic energy and the decrease in the turbulent kinetic energy near the ground. The hit rates of gust wind speeds in the vertical planes predicted by the proposed and W&O models are 0.93 and 0.71, while the hit rates of gust wind speeds in the horizontal planes predicted by the two models are 0.96 and 0.64. It is obvious that the proposed model shows higher hit rates in the vertical and horizontal planes compared to the W&O model.

To evaluate the performance of the two models in regions with flow separation and reattachment, Fig. 17 presents the predicted gust wind speeds normalized by those from the LES simulation at four representative points around the single building, namely points A, B, C and D as shown in Fig. 15 (c). As mentioned by Tominaga [21], the wind field around a single building is characterized by the reattachment length at the rooftop and behind the building. Point A is chosen to evaluate the gust wind speed near the reattachment region. Points B and D are in the wake region of the single building. The former is closer to the building and the wake effect is more severe, while the latter is also affected by the wake, but the wake effect is weaker than point B. In addition, point C near the ground is selected to investigate the interaction between the single building and the ground. The proposed model can accurately predict the gust wind speed with the relative error of less than 5 %, while the W&O model shows an observable underestimation in the wake region with the relative error of about 14 %. In this study, the correction coefficient $f(t_{ave}/t_{tot})$ is proposed for different averaging times and is first validated by the most severe case of t_{ave} = 10 s. The cases of t_{ave} = 5 s and t_{ave} = 3 s are also validated and show good agreement with the LES results.

The validation metrics of skewness and kurtosis by the proposed modified Hermite model and W&O model in the vertical and horizontal planes are presented in Fig. 18. In the vertical plane shown in Fig. 18 (a) and (b), the skewness at most selected points obtained by the proposed

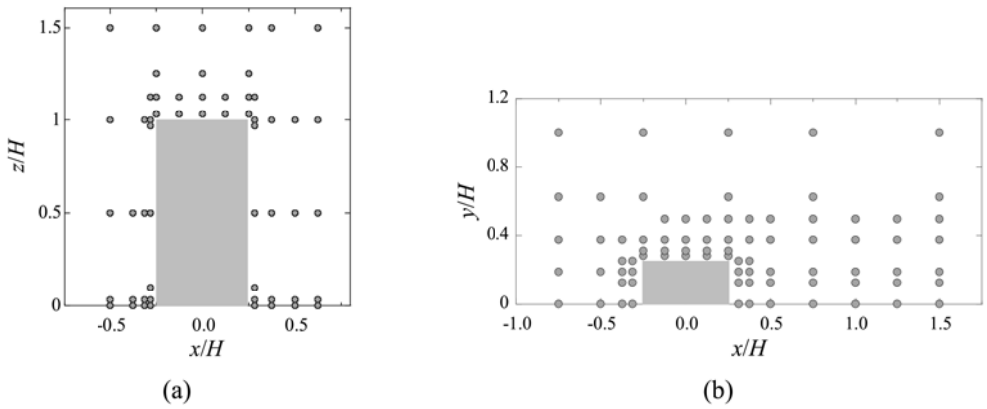

Fig. 14. Distribution of selected points around the single building on the (a) vertical plane of $y/H = 0$ and (b) horizontal plane of $z/H = 0.0625$ to record instantaneous wind velocity.

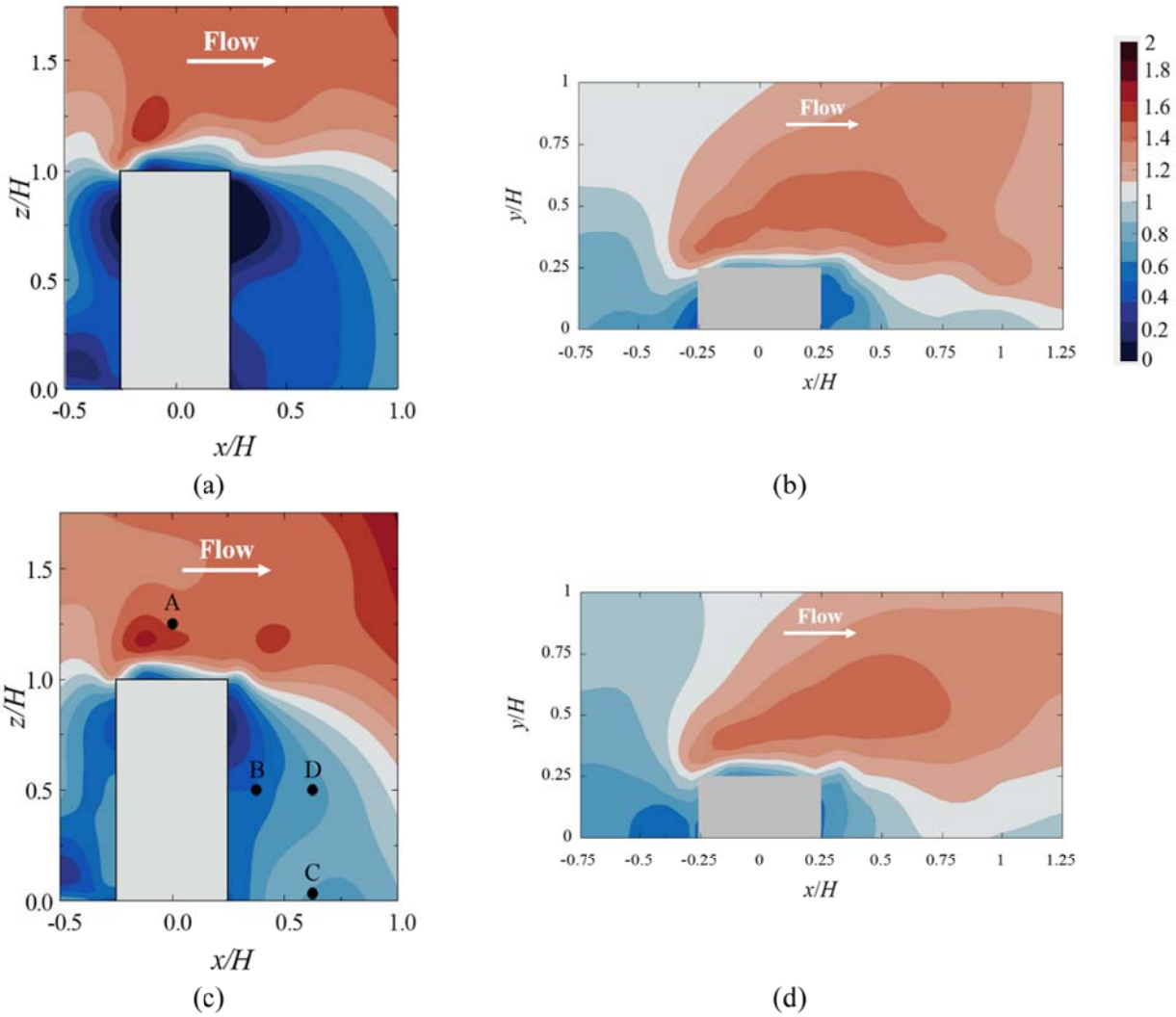

Fig. 15. Comparison of contours of gust factors around the single building. (a, b) Predicted gust factors by LES on the vertical plane of $y/H = 0$ and the horizontal plane of $z/H = 0.0625$. (c, d) Predicted gust factors by the proposed model with $t_{ave} = 10$ s on the vertical plane of $y/H = 0$ and the horizontal plane of $z/H = 0.0625$.

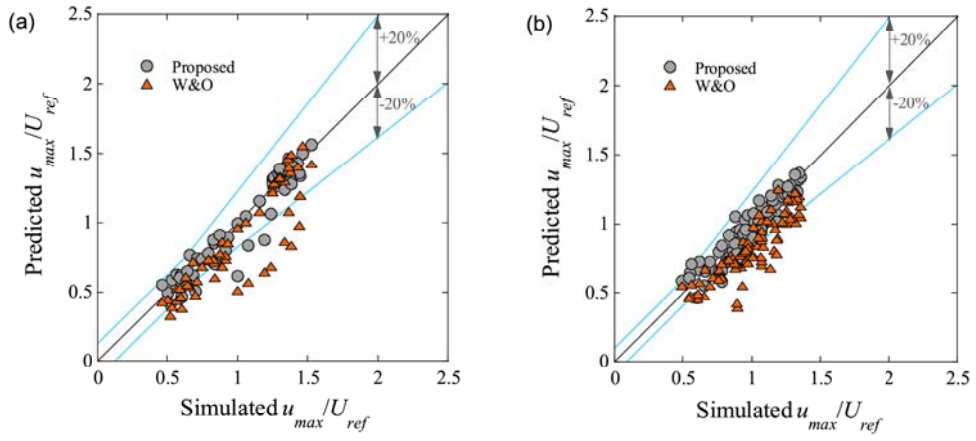

Fig. 16. Validation metrics of normalized gust wind speed around the single building by the proposed model with $t_{ave} = 10$ s and W&O model on (a) the vertical plane of $y/H = 0$ and (b) the horizontal plane of $z/H = 0.0625$.

modified Hermite model and W&O model are within the borderlines of the validation metrics. The hit rates of skewness predicted by the proposed model and the W&O model are 0.93 and 0.93, while the hit rates of kurtosis predicted by the two models are 0.84 and 0.77. However, in the horizontal plane as shown in Fig. 18 (c) and d, the two models show slight underestimations. The hit rates of skewness predicted by the proposed model and the W&O model are 0.90 and 0.75, while the hit rates of kurtosis predicted by the two models are 0.89 and 0.78. In

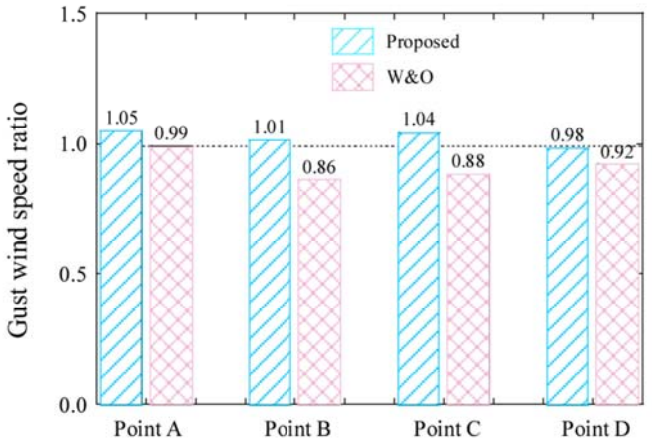

Fig. 17. Comparison of predicted gust wind speed ratio at four representative points A, B, C and D around the single building shown in Fig. 15 (c) by the proposed model with t_{ave} = 10 s and W&O model.

general, predictions from the W&O model are more horizontally aligned, while those from the proposed model are more diagonally distributed. A similar trend in the gust factors was also reported in Wang and Okaze [20]. The reason for the horizontal alignment of the results from the W&O model is that the shape parameter of Weibull distribution involved in the calculation of skewness and kurtosis is overestimated. On the other hand, the skewness and kurtosis from the proposed model are calculated based on the time series of velocities, so they are closer to the LES results.

4. Conclusions

In this study, a novel unsteady Reynolds-Averaged Navier-Stokes (URANS) model with a prespecified averaging time and turbulent inflow is proposed. A new peak factor is derived to consider the effect of averaging time used in URANS. The gust wind speeds over flat terrain and around a single building predicted using the URANS and the proposed peak factor are validated by LES simulations. The following conclusions are obtained.

1. A novel URANS is proposed in conjunction with a prespecified averaging time and turbulent inflow. The mean wind speed, standard deviation, skewness and kurtosis with different averaging times are examined. The first four moments are almost independent of the averaging time up to 10 s. This characteristic reduces the computational time to predict gust wind speeds using URANS.
2. A new peak factor based on Hermite model is proposed to consider the effect of the averaging time. The variation of zero-crossing rate with the averaging time is investigated first and then a correction coefficient is proposed, which shows good agreement with those by LES simulations.
3. The gust wind speeds predicted using URANS and the new peak factor over flat terrain and around a single building are validated by LES simulations. For flat terrain, the gust wind speeds predicted by the proposed model are in good agreement with those obtained by

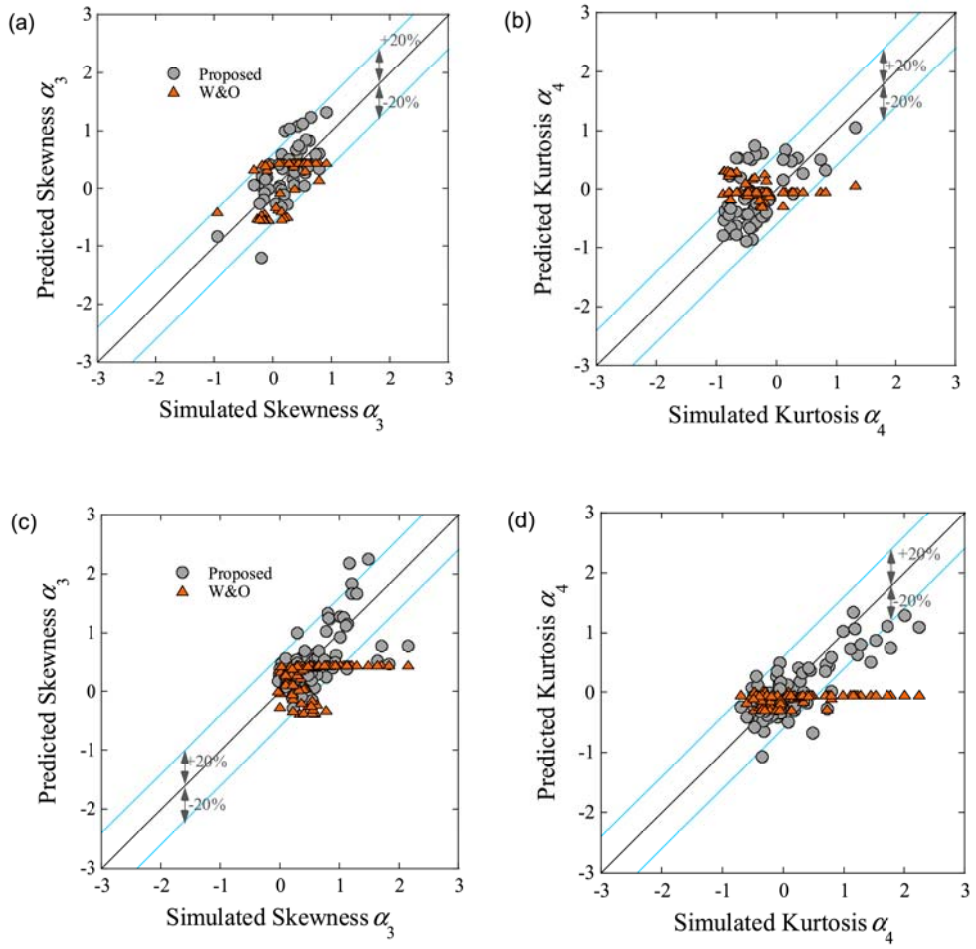

Fig. 18. Validation metrics of (a, c) skewness on the vertical plane of $y/H = 0$ and the horizontal plane of $z/H = 0.0625$ and (b, d) kurtosis on the vertical plane of $y/H = 0$ and the horizontal plane of $z/H = 0.0625$ by the proposed model with t_{ave} = 10 s and W&O model.

LES, while the Akahoshi model shows an overestimation, and the W&O model presents an underestimation. For the single building, most of the gust wind speed predicted by URANS and the new peak factor are well captured even in regions with flow separation and reattachment, while those from the W&O model are underestimated near the top of building and overestimated in the wake region.

In this study, the proposed method shows superior performance compared to conventional models, but validation for a wide range of turbulent flows is expected. In addition, the correction coefficient is proposed as a function of t_{ave}/T_{tot} since the same grid size is used in the LES and URANS simulations. However, the grid resolution may affect the correction coefficient, and further optimization with respect to the grid size is expected in future studies.

Additional information

The authors declare no competing interests

CRediT authorship contribution statement

Xiangyan Chen: Writing – original draft, Visualization, Software, Investigation, Formal analysis, Data curation. **Takeshi Ishihara:** Writing – review & editing, Validation, Supervision, Resources, Methodology, Conceptualization.

Declaration of competing interest

The authors declare that they have no known competing financial interests or personal relationships that could have appeared to influence the work reported in this paper.

Acknowledgments

This research is carried out as part of a joint program for next generation energy infrastructure with Toshiba Energy Systems & Solutions Corporation, J-POWER, Shimizu Corporation, Class NK, Tokyo Gas, CHOBU Electric Power. The authors express their deepest gratitude to the concerned parties for their assistance during this study. The authors also wish to thank the China Scholarship Council (Grant No. CSC202006130016) for the funding support

Appendix A. Prediction of gust wind speeds by Akahoshi model

Akahoshi et al. [19] analyzed measurement data from 67 sites and used the turbulence intensity I_u to approximate α_3 and α_4 in Eqs. (A. 1) and (A. 2) as:

$$\alpha_3 = 3I_u\left[-0.8\left(\frac{h}{250}\right)+0.5\right] \tag{A. 1}$$

$$\alpha_4 = \alpha_3^2 + 3 \tag{A. 2}$$

where α_3 is in the range -1 $\leq \alpha_3 \leq$ 1. h is the height above the ground and is less than 250 m.

Akahoshi et al. [19] also expressed κ in Eq. (A. 3) as 1 and X in Eq. (A. 4) is a function of the turbulence intensity,

$$\kappa = 1 \tag{A. 3}$$

$$X = 0.39I_u + 2.54 \tag{A. 4}$$

Since the higher-order moments in Eqs. (A. 1)–(A. 3) and X in Eq. (A. 4) are approximated as functions of the turbulence intensity, the gust wind speeds can be calculated by Eq. (17) if the mean wind speed and turbulence intensity are obtained from numerical simulations. The Akahoshi model is used to predict gust wind speeds for almost 3 s over flat terrain.

Appendix B. Prediction of gust wind speeds by W&O model

Wang and Okaze [20] investigated the gust wind speed $u_{max,q}$ around an isolated building and a building array using the mean velocity U and the standard deviation σ_u as:

$$u_{max,q} = G_{max,q}U = \frac{[-\ln(q)]^{1/\beta}}{\Gamma(1+1/\beta)}U \tag{B. 1}$$

where $G_{max,q}$ is the gust factor with the exceedance probability of q, which is defined by users as illustrated by Ikegaya et al. [43] and can be determined by normal distribution when it ranges between 10 % and 90 %. β is the shape parameter of two-parameter Weibull distribution and approximated as:

$$\beta = 9.6\exp\left(-12.2\frac{k}{k+K}\right)+2.3 \tag{B. 2}$$

where the kinetic energy ratio $k/(k+K)$ is used to represent the characteristics of wind fields. Both turbulent kinetic energy k and mean kinetic energy K are expressed as:

$$k = \frac{1}{2}\left(\sigma_u^2+\sigma_v^2+\sigma_w^2\right) \tag{B. 3}$$

$$K = \frac{1}{2}\left(U^2+V^2+W^2\right) \tag{B. 4}$$

where σ_u^2, σ_v^2 and σ_w^2 are the squared standard deviations in the streamwise, spanwise and vertical directions. U, V and W are the mean velocities in the corresponding directions, respectively.

In the W&O model, skewness α_3 and kurtosis α_4 are derived based on the two-parameter Weibull distribution and expressed as:

$$\alpha_3 = \frac{\Gamma(1+3/\beta) - 3\Gamma(1+2/\beta)\Gamma(1+1/\beta) + 2\Gamma^3(1+1/\beta)}{[\Gamma(1+2/\beta) - \Gamma^2(1+1/\beta)]^{3/2}} \tag{B.5}$$

$$\alpha_4 = \frac{\Gamma(1+4/\beta) - 4\Gamma(1+3/\beta)\Gamma(1+1/\beta) + 6\Gamma(1+2/\beta)\Gamma^2(1+1/\beta) - 3\Gamma^4(1+1/\beta)}{[\Gamma(1+2/\beta) - \Gamma^2(1+1/\beta)]^2} \tag{B.6}$$

where Γ is the gamma function.

Similar to Akahoshi model, the W&O model also presented higher-order moments of velocity based on lower-order moments, i.e., the mean velocities and the standard deviations of the fluctuating velocities. The W&O model with the exceedance probability q of 10 % is used to predict gust wind speeds for almost 3 s over flat terrain and around a single building if the mean wind speed and turbulence intensity are obtained from numerical simulations.

Data availability

Data will be made available on request.

References

[1] G. Liu, X. Wang, Q. Wu, D. Fang, Z. Wu, H. Liu, M. Lyu, Effect of urbanization on gust wind speed in summer over an urban area in Eastern China, Environ. Res. Lett. 18 (2023) 1–9, https://doi.org/10.1088/1748-9326/acddfa.

[2] L. Kristensen, M. Casanova, M.S. Courtney, I. Troen, In search of a gust definition, Bound. Layer Meteorol. 55 (1) (1991) 91–107, https://doi.org/10.1007/BF00119328.

[3] W. Zhou, D. Zhang, M. Yang, Analysis of extreme operating gust influence on aerodynamic performance of wind turbine, in: Proceedings of the 4th International Academic Exchange Conference on Science and Technology Innovation, Guangzhou, 2022, pp. 9–13, https://doi.org/10.1109/IAECST57965.2022.10062279.

[4] J. Wang, G.A. Kopp, Gust effect factors for windward walls of rigid buildings with various aspect ratios, J. Wind Eng. Ind. Aerodyn. 212 (2021) 1–21, https://doi.org/10.1016/j.jweia.2021.104603.

[5] IEC 61400-1, Wind energy generation systems-Part 1: design requirements, in: Edition 4, International Electrotechnical Commission, 2019.

[6] J.D. Holmes, A.C. Allsop, J.D. Ginger, Gust durations, gust factors and gust response factors in wind codes and standards, Wind Struct. 19 (3) (2014) 339–352, https://doi.org/10.12989/was.2014.19.3.339.

[7] World Meteorological Organization, Measurement of surface wind. Guide to Meteorological Instruments and Methods of Observation, WMO-No. 8, 7th ed., World Meteorological Organization, Geneva, Switzerland, 2008.

[8] T. Burton, D. Sharpe, N. Jenkins, E. Bossanyi, Wind Energy Handbook, John Wiley & Sons, New York, 2011.

[9] M. Hino, On the gust factor-Relationship between the instantaneous maxima and averaging and sampling times, in: Proceedings of the 14th Japan National Congress for Applied Mechanics, 1965, pp. 132–139.

[10] N. Ikegaya, Y. Ikeda, A. Hagishima, J. Tanmoto, Statistical analysis of wind speeds at a pedestrian level of urban-like roughness, J. Wind Eng. 42 (2017) 1–8, https://doi.org/10.5359/jwe.42.1 (in Japanese).

[11] H. Kikumoto, T. Okaze, N. Ikegaya, Y. Tominaga, Investigating statistics of peak wind speed around an isolated building model via large-eddy simulation, in: Proceedings of the Fifteenth International Conference on Wind Engineering, Beijing, China, 2019, pp. 311–312. September 1-6, 2019.

[12] T.W.C. Luis. Numerical simulation of the dynamics of turbulent swirling flames, Dissertation, Technische Universität München, GER, 2012. https://www.epc.ed.tum.de/fileadmin/w00cgc/tfd/Forschung/Dissertationen/Tay_2012_Numerical_Simulation_of_the_Dynamics_of_Turbulent_Swirling_Flames.pdf.

[13] J. Weiringa, Gust factors over open water and built-up country, Bound. Layer Meteorol. 3 (1973) 424–441, https://doi.org/10.1007/BF01034986.

[14] H. Ishizaki, Wind profiles, turbulence intensities and gust factors for design in typhoon-prone regions, J. Wind Eng. Ind. Aerodyn. 13 (1-3) (1983) 55–66, https://doi.org/10.1016/0167-6105(83)90128-9.

[15] Y. Misu, T. Ishihara, Prediction of frequency distribution of strong crosswind in a control section for train operations by using onsite measurement and numerical simulation, J. Wind Eng. Ind. Aerodyn. 174 (2018) 69–79, https://doi.org/10.1016/j.jweia.2017.11.020.

[16] A.G. Davenport, Note on the distribution of the largest value of a random function with application to gust loading, Proc. Inst. Civ. Eng. 28 (2) (1964) 187–196, https://doi.org/10.1680/iicep.1964.10112.

[17] S.R. Winterstein, Moment-Based Hermite Models of Random Vibration, Technical Univercity of Denmark, Denmark, 1987, pp. 1–29, https://doi.org/10.13140/RG.2.2.29938.56004. Department of Structural Engineering.

[18] D.K. Kwon, A. Kareem, Peak factors for non-Gaussian load effects revisited, J. Struct. Eng. 137 (2011) 1611–1619, https://doi.org/10.1061/(ASCE)ST.1943-541X.0000412, 2011.

[19] A. Akahoshi, A. Sarukawa, R. Sasaki, K. Miyashita, O. Nakamura, Y. Uematsu, Study of relation between peak factor and turbulence intensity by using the wind observation data at various locations, J. Wind Eng. 42 (2017) 134–143, https://doi.org/10.5359/jwe.42.134 (In Japanese).

[20] W. Wang, T. Okaze, Estimating low-occurrence wind speeds from mean velocity and turbulent kinetic energy: development of statistical method and validation with idealized cases, Build. Environ. 224 (2022) 1–16, https://doi.org/10.1016/j.buildenv.2022.109499.

[21] Y. Tominaga, Flow around a high-rise building using steady and unsteady RANS CFD: Effect of large-scale fluctuations on the velocity statistics, J. Wind Eng. Ind. Aerodyn. 142 (2015) 93–103, https://doi.org/10.1016/j.jweia.2015.03.013.

[22] T. Ishihara, Y. Qi, Numerical study of turbulent flow fields over steep terrain by using modified delayed detached-eddy simulations, Bound. Layer Meteorol. 170 (1) (2019) 45–68, https://doi.org/10.1007/s10546-018-0389-8.

[23] L. Xu. Second generation unsteady Reynolds Averaged Navier Stokes approach for application to aerodynamic design and optimization in the automotive industry, Dissertation, Massachusetts Institute of Technology, Massachusetts, USA, 2020.. https://dspace.mit.edu/handle/1721.1/127734.

[24] Fluent. Ansys Fluent Theory Guide, Ansys Inc, 2021. https://dl.cfdexperts.net/cfd_resources/Ansys_Documentation/Fluent/Ansys_Fluent_Theory_Guide.pdf.

[25] V. Yakhot, S.A. Orszag, S. Thangam, T.B. Gatski, C.G. Speziale, Development of turbulence models for shear flows by a double expansion technique, Phys. Fluids 4 (1992) 1510–1520, https://doi.org/10.1063/1.858424.

[26] J García, J Munoz-Paniaguaa, L Xu, E Bagliettob, A second-generation URANS model (STRUCT-ε) applied to simplified freight trains, J. Wind Eng. Ind. Aerodyn. 205 (2020) 1–11, https://doi.org/10.1016/j.jweia.2020.104327.

[27] J. Feng, L. Xu, E. Baglietto, Assessing the applicability of the structure-based turbulence resolution approach to nuclear safety-related issues, Fluids 6 (61) (2021) 1–14, https://doi.org/10.3390/fluids6020061.

[28] K. Enoki, T. Ishihara, A generalized canopy model and its application to the prediction of urban wind climate, J. Jpn. Soc. Civ. Eng. Ser. A1 Struct. Eng. Earthq. Eng. 68 (1) (2012) 28–47, https://doi.org/10.2208/jscejseee.68.28 (In Japanese).

[29] T. Ishihara, G.W. Qian, Y.H. Qi, Numerical study of turbulent flow fields in urban areas by using modified k-ε model and large eddy simulation, J. Wind Eng. Ind. Aerodyn. 206 (2020) 1–20, https://doi.org/10.1016/j.jweia.2020.104333.

[30] Y. Meng, K. Hibi, Turbulent measurements of the flow field around a high-rise building, J. Wind Eng. (76) (1998) 55–64, https://doi.org/10.5359/jawe.1998.76_55, 1998(In Japanese).

[31] H. Irwin, Design and use of spires for natural wind simulation, J. Wind Eng. Ind. Aerodyn. 7 (3) (1981) 361–366, https://doi.org/10.1016/0167-6105(81)90058-1.

[32] Y. Qi, T. Ishihara, Numerical study of turbulent flow fields around of a row of trees and an isolated building by using modified k-ε model and LES model, J. Wind Eng. Ind. Aerodyn. 177 (2018) 293–305, https://doi.org/10.1016/j.jweia.2018.04.007.

[33] AIJ. AIJ recommendations for loads on buildings, Architectural Institute of Japan, 2019.

[34] M.D. Israel, The myth of URANS, J. Turbul. 24 (8) (2023) 367–392, https://doi.org/10.1080/14685248.2023.2225140.

[35] J. Jeong, F. Hussain, On the identification of a vortex, J. Fluid Mech. 285 (1995) 69–94, https://doi.org/10.1017/s0022112095000462, 1995.

[36] M. Schatzmann, H. Olesen, J. Franke, COST 732 Model Evaluation Case Studies: Approach and Results, COST Office, Brussels, 2010, p. 121.

[37] D. Oettl, Quality assurance of the prognostic, microscale wind-field modelGRAL14.8 using wind-tunnel data provided by the German VDI guideline 3783-9, J. Wind Eng. Ind. Aerodyn. 142 (2015) 104–110, https://doi.org/10.1016/j.jweia.2015.03.014.

[38] S. Seng, C. Monroy, S. Malenica, On the use of Euler and Crank-Nicolson time stepping schemes for seakeeping simulations in OpenFOAM, in: Proceedings of the Seventh International Conference on Computational Methods in Marine Engineering, Nantes, France, 2017 (MARINE 2017)May 15-17, 2017, https://upc

ommons.upc.edu/bitstream/handle/2117/332090/Marine-2017-74_ON%20THE%20USE%20OF%20EULER.pdf.

[39] K.A. Hadi, J.R. Mohammed, A.Q. Jawad, A.I. Kheioon, Simulation of flow around circular cylinders for complex von Karman vortex street phenomenon using SIMPLE, SIMPLEC and PISO, Basrah J. Eng. Sci. 24 (2) (2024) 43–49, https://doi.org/10.33971/bjes.24.2.6.

[40] R. Courant, K. Friedrichs, H. Lewyt, On the partial difference equations of mathematical physics, IBM J. Res. Dev. 11 (2) (1967) 215–234, https://doi.org/10.1147/rd.112.0215.

[41] M. Shirzadi, Y. Tominaga, CFD evaluation of mean and turbulent wind characteristics around a high-rise building affected by its surroundings, Build. Environ. 225 (2022) 109637, https://doi.org/10.1016/j.buildenv.2022.109637.

[42] W. Li, M.C. Mak, C. Cai, Y. Fu, T.K. Tse, J. Niu, Wind tunnel measurement of pedestrian-level gust wind flow and comfort around irregular lift-up buildings within simplified urban arrays, Build. Environ. 256 (2024) 111487, https://doi.org/10.1016/j.buildenv.2024.111487.

[43] N. Ikegaya, T. Kawaminami, T. Okaze, A. Hagishima, Evaluation of exceeding wind speed at a pedestrian level around a 1:1:2 isolated block model, J. Wind Eng. Ind. Aerodyn. 201 (2020) 104193, https://doi.org/10.1016/j.jweia.2020.104193.